IOP Publishing Journal of Optics
J. Opt. 16 (2014) 065006 (7pp) doi:10.1088/2040-8978/16/6/065006

Fabrication of long-range surface plasmon polaritons waveguide by wet chemical etching

Ying Xie[2], Tong Liu[2], Xuliang Zhao[2], Meiling Zhang[2], Changming Chen[1,2], Fei Wang[1,2], Xiaoqiang Sun[1,2] and Daming Zhang[1,2]

[1] State Key Laboratory on Integrated Optoelectronics, Jilin University, Changchun, Jilin 130012, People's Republic of China
[2] College of Electronic Science & Engineering, Jilin University, Changchun, Jilin 130012, People's Republic of China

E-mail: sunxq@jlu.edu.cn

Received 25 March 2014, revised 22 April 2014
Accepted for publication 23 April 2014
Published 29 May 2014

Abstract

The fabrication of long-range surface plasmon polaritons (LRSPPs) waveguides based on a thin Au stripe embedded in poly(methyl-methacrylate-glycidly-methacrylate) polymers was investigated. By patterning the photoresist, a wet chemical etching technique was used to avoid sharp pin-like and shark-fin-like structures on the edges of the Au stripe. The surface morphology of the Au film and polymer cladding were studied by atomic force microscopy (AFM), as well as by using the waveguide configuration of the Au stripe. AFM images proved the elimination of parasitic structures. A 2 cm long, 4 μm wide, and 25 nm thick Au stripe waveguide exhibited a propagation loss of approximately 4.3 dB cm^{-1} measured by the cut-back method and end-fire excitation of LRSPP mode guiding at 1550 nm. The demonstration of optical signal transmission indicates that the LRSPP waveguide fabricated by wet chemical etching is a potential solution to on-chip optical interconnections.

Keywords: long-range surface plasmon polaritons, polymer, wet chemical etching

(Some figures may appear in colour only in the online journal)

1. Introduction

For high-capacity information transmissions, the bottleneck has shifted from processors to bandwidths due to the inherent limitation of electrical copper lines. Optical interconnects that can provide wider bandwidths and good resistance to electromagnetic interference have become a promising solution, even though the electrical interconnects are still developing rapidly [1]. Different technological solutions and material systems, such as III-V semiconductors, silica, silica-on-silicon, silicon oxynitride, and lithium niobate crystals have been well investigated for the application of optical interconnects [2–5]. Due to characteristics of low cost, easy fabrication, and flexibility, polymers are widely used for optical routing in different devices [6]. Recently, plasmonic structures with thin metal stripes embedded in polymer materials have exhibited potential in the application of splitters, modulators, switches, gratings, attenuators, and chip-to-chip or board-to-board interconnects [7–13]. Surface plasmon polaritons (SPPs) are waves of longitudinal charge oscillations of the conduction of electrons at the metal surface. A transverse magnetic (TM) polarized optical surface wave can propagate along the interface between a metal and a dielectric. SPPs have high confinement and sensitivity; however, they decay exponentially into both media with a small penetration depth due to the internal damping in metal, which limits the propagation distance [14–16]. When a thin metal film with a finite width is embedded in a homogeneous dielectric, it can support a fundamental and symmetrical mode propagation, which is called long-range SPPs (LRSPPs) [17, 18]. Compared with dielectric-metal single-interface SPPs, the centimeters-long propagation of LRSPP waveguides offers the potential to be an optical or electrical signal transmission line interconnecting element due to its low attenuation [14, 15]. Metal stripes

with different widths and thicknesses can provide various mode field diameters of several micrometers, which facilitate the optical excitation by a single mode (SM) fiber and decreases the coupling loss [19]. However, because of the symmetry request and the tightly restrained mode, the optical loss of LRSPP waveguides is highly sensitive to interface conditions [20].

The fabrication of metal stripes on polymer cladding by conventional single-step liftoff methods will lead to the formation of sharp pin-like and shark-fin-like structures on the edges of the metal stripe, which is unfavorable to mode control and increases optical loss [21]. A double-layered liftoff process is used to form an overhanging structure to overcome this obstacle [22]. However, with this method, a buffered SiN_x layer needs to be formed on the polymer cladding layer by chemical vapor deposition. Development and wet etching are required to remove the photoresist and SiN_x, respectively, which complicates the fabrication process. The buffered oxide etchant may damage the surface morphology of the polymer cladding and result in refractive index (RI) asymmetry around the metal stripe. Therefore, a simple fabrication process that can provide a favorable metal stripe configuration without parasitic structures needs to be developed.

In this paper, wet chemical etching and photolithography processes were used to fabricate Au stripe LRSPP waveguides. Defects of shark-fin-like structures on the edges of the metal stripe were eliminated by a photoresist mask. Using the cross-sectional view of an atomic force microscope (AFM) image, a quasi-rectangular waveguide configuration was obtained. The RI and roughness properties of poly(methylmethacrylate-glycidly-methacrylate) (P(MMA-GMA)) cladding were characterized. The optical characteristics of fabricated waveguides were investigated using end-fire excitation of LRSPP mode guiding at 1550 nm.

2. Experiment

2.1. Process concept

Traditional liftoff methods that form a metal stripe on polymer cladding remove the unnecessary part of the evaporated metal film by wiping off the photoresist. Due to the excessive accumulation of metal along the sidewalls of the photoresist, imperfect shark-fin-like overhanging structures on the edges of the metal stripe will form [21]. Moreover, ultrasonic liftoff processes demand that the metal stripe should have good adhesion to the polymer cladding to prevent it from peeling off with the photoresist [23, 24]. For some polymer claddings, the photoresist is hard to be removed cleanly. The solvent in the photoresist may also erode the polymer cladding. These passive effects will break the symmetry of RI around the metal stripe, which is crucial for the formation of an LRSPP mode [25].

To solve the above problems and improve the optical performance of LRSPP waveguides, we adopted the photoresist, which is patterned by photolithography, as the mask of metal stripe. Wet chemical etching is used to remove the metal film without the protection of the photoresist. Figure 1 presents the schematic diagram of the fabrication process. With this method, a steep sidewall of metal stripe without parasitic microstructures can be obtained. No passive effects, such as polymer surface roughening or solvent erosion, will be induced by Au deposition or metal removal by wet etching. This is a result of the protection of the Au film that exists between the photoresist and cladding. Moreover, the adhesion between the under and upper cladding layers will also be enhanced.

2.2. Au stripe fabrication

First, a layer of 15 μm thick P(MMA-GMA) was spin-coated on a silicon wafer at 2500 rpm as the lower cladding. After a subsequent bake at 120 °C for 2.5 h, a thermal evaporation method was used to deposit high-purity (>99.999%) solid Au thin metal film onto the polymer cladding. A calibrated quartz-crystal microbalance as the thickness monitor was used to keep the deposition at a rate of 0.05 nm s^{-1} to control the thickness. The photoresist BP212 (Kempur Microelectronics Inc., China) was spin-coated and patterned by an ultraviolet (UV) photolithography machine (ABM Co. Inc., USA) to define waveguide patterns on the Au film. The solution of KI: I_2: H_2O = 4:1:100 was used to wipe off the metal film without the protection of the photoresist. After that, the sample was exposed to UV light and immersed in 1 wt% NaOH solution, agitated to remove the photoresist introduced in the fabrication process. Subsequently, the same P(MMA-GMA) material was spin-coated and cured on the Au stripe as the upper cladding. Before measurement, the waveguide sample was sliced by a wafer-dicing machine DAD-3220 (DISCO Co. Inc., Japan) to minimize the uncertainty of input/output coupling losses.

2.3. Meaturement

The schematic diagram of the transmission characteristics measurement setup of LRSPP waveguides is shown in figure 2. The fiber tips were cleaned and checked to ensure they were in good condition. The end-fire excitation of the LRSPP mode guiding at telecommunication wavelengths along thin Au stripes with finite widths embedded in dielectric has been experimentally proven [17]. Thus, the light from a tunable laser source TSL-210 (Santec Co., Japan) at a wavelength of 1550 nm, which was modulated by a sinusoidal electrical signal from the generator SP1461 (Sample Instrument Co. Ltd., China) through an electro-optic modulator LN56S (Thorlabs Inc., USA), was perpendicularly polarized to the waveguide plane by passing it through a polarization controller and then launching it into the waveguide to excite an LRSPP mode. A standard SM fiber was used to couple the output signal to an optical power meter or a photo receiver. The output fiber alignment was optimized with a five-axis position control to maximize the optical output of the LRSPP mode, so did the input fiber alignment, until the best conditions were achieved. The far-field output of the Au stripe waveguide was monitored by an infrared (IR) camera with

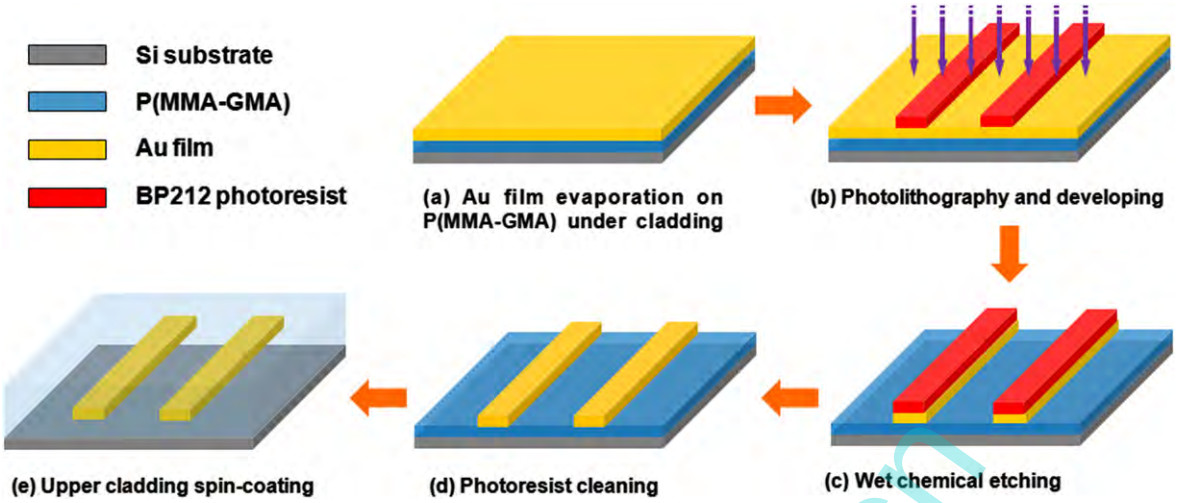

Figure 1. Schematic diagram of the proposed wet chemical etching process to fabricate the Au stripe LRSPP waveguide.

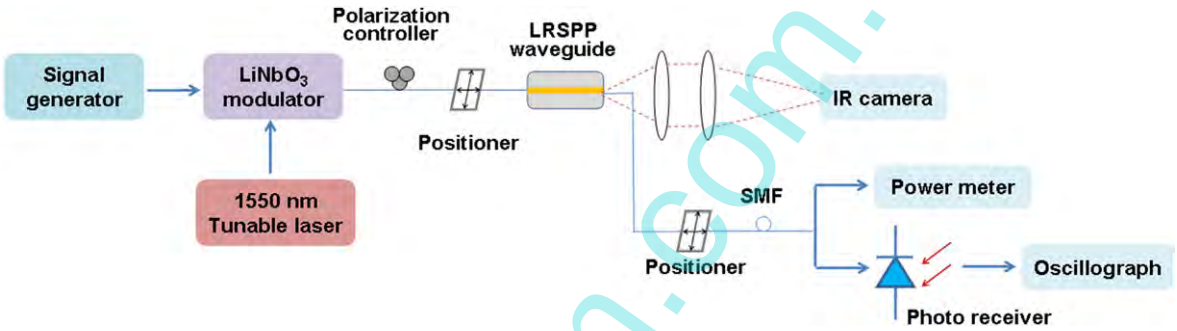

Figure 2. Schematic setup for characterizations of insertion loss, optical signal transmission, and far-field output pattern of LRSPP waveguide.

200 magnifications. The optical transmission property of the fabricated LRSPP waveguide was measured by an oscilloscope that collected the output optical power with the butt-coupled SM fiber [26].

3. Characterization

3.1. P(MMA-GMA) cladding

The P(MMA-GMA) material we synthesized is used as the polymer cladding in this study due to its desirable characteristics of low dispersion coefficient, ease of fabrication, and low cost [27]. Figure 3 shows the RI of P(MMA-GMA) as a function of wavelengths, measured by an ellipsometer M-2000UI (J A Woollam Co. Inc., USA) from the average of three different samples. After 3 h baking, the RI of film was 1.4802 for TM polarization at 1550 nm. This low RI cladding is favorable to reducing the optical loss due to its relatively weak mode control. In addition, the optical stability of P(MMA-GMA) was verified experimentally to guarantee the crucial RI symmetry requirement of the LRSPP waveguide. The results show that the fluctuation of RI is less than 3×10^{-4} during 8 h baking at 120 °C, which is solid enough for cladding application.

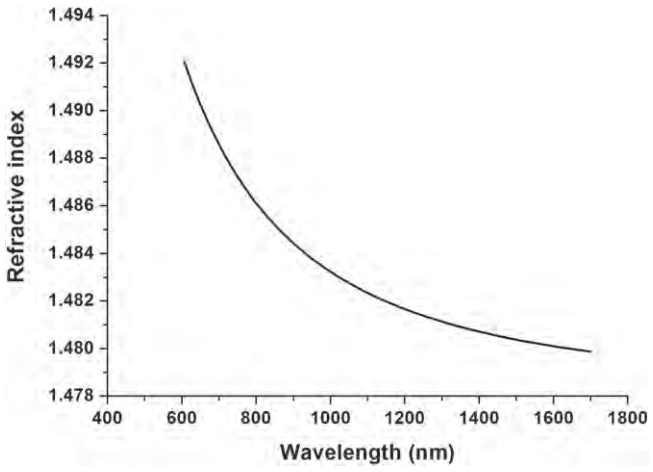

Figure 3. RI of the P(MMA-GMA) cladding material as a function of wavelengths.

The absorption property of P(MMA-GMA) was characterized by a spectrophotometer UV 3600 (SHIMADZU Co., Japan) over a wavelength range of 300–1700 nm, as shown in figure 4. The low absorbance of P(MMA-GMA) at 1550 nm implies a favorable property to reduce optical loss. In fact, the propagation loss of a rectangular P(MMA-GMA) waveguide measured by cut-back method is 2 dB cm^{-1} at

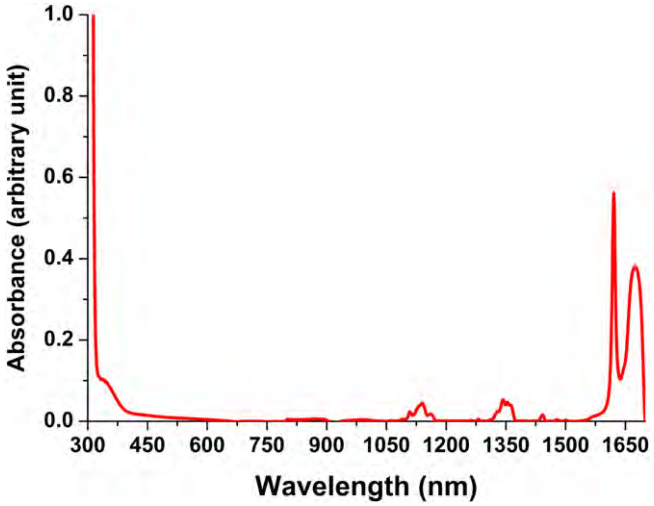

Figure 4. UV-Vis-NIR absorption spectrum of P(MMA-GMA) after thermal curing.

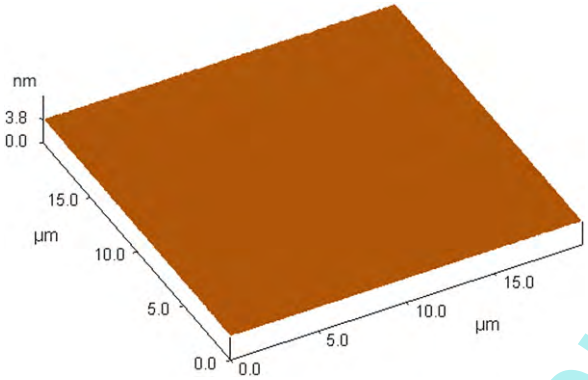

Figure 5. AFM image of the P(MMA-GMA) cladding with a RMS roughness of 0.3 nm.

1550 nm with a core-cladding index contrast of 0.6%. Compared with that of ZPU12 series polymer [28], this larger propagation loss is mainly induced by the material absorption difference between ZPU12 resins and P(MMA-GMA) material. To examine the surface morphology of cladding before Au deposition, AFM images of P(MMA-GMA) film were recorded with a multimode scanning probe microscope CSPM5000 (Being Nano-Instrument Ltd., China) that operated in contact mode, as shown in figure 5. It can be seen that the root-mean-square (RMS) roughness is just 0.3 nm on a $20 \times 20\ \mu m^2$ area, which is smooth enough for the demand of LRSPP waveguide cladding to avoid roughness-induced scattering loss and ohmic loss of metal stripe.

3.2. Au film

The Au film thickness and roughness has significant impact on the resistivity of Au film, because electrons scattering on a rough film surface will result in a resistivity increment of larger than the bulk value [29]. According to the Drude model, the waveguide attenuation changes with the metal film resistivity. Therefore, surface roughness becomes a key issue to minimize the optical loss [30]. As has been reported, discontinuous and

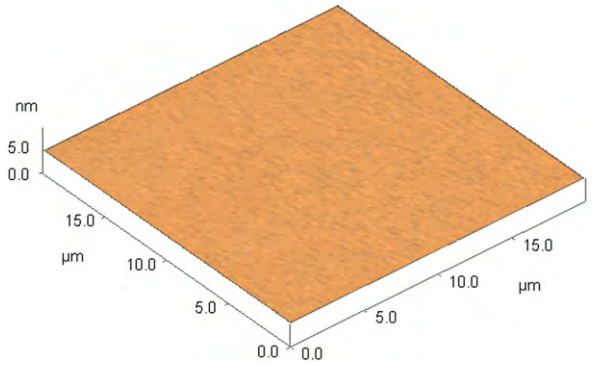

Figure 6. AFM image of the Au film surface morphology with a RMS roughness of 1.2 nm on P(MMA-GMA) cladding after thermal evaporation.

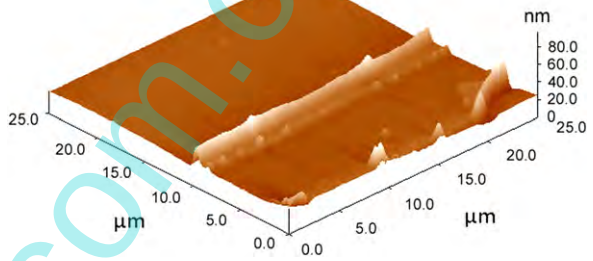

Figure 7. AFM image of the Au stripe fabricated by the conventional liftoff method.

highly islandized films may be formed as depositing very thin metal films [31]. Thus, the deposition parameters, such as electrical current and vacuum condition, need to be optimized to improve the quality of thin Au film. Figure 6 shows the AFM image of Au film surface morphology on P(MMA-GMA) cladding after thermal evaporation. The smooth surface with a low RMS roughness value of 1.2 nm can be observed. Based on theoretical results from Kuan *et al* [32] the resistivity increment due to this amplitude is less than 10%, which will not bring remarkable passive impact on the optical loss. As a contrast, for some claddings like CYTOP, plasma-etching pretreatment is needed to enhance the adhesion of the Au film, which will inevitably affect the surface roughness of metal film and, consequently, the waveguide attenuation [33]. Here, the Au film can be directly deposited on the P(MMA-GMA) surface without any pretreatment and maintains good adhesion, which facilitates the waveguide fabrication.

3.3. Au stripe

To evaluate the proposed process, a metal stripe was first fabricated by the conventional liftoff method [21]. From the AFM image characterization shown in figure 7, shark-fin-like structures on the edges of the Au stripe can be seen, which is unacceptable for the application of LRSPP waveguides. To demonstrate the morphological details of surface and sidewall roughness of the Au stripe fabricated by the wet chemical etching process, an AFM machine Dimension Icon (Bruker Co., USA) with a better solution was adopted. Figure 8 shows

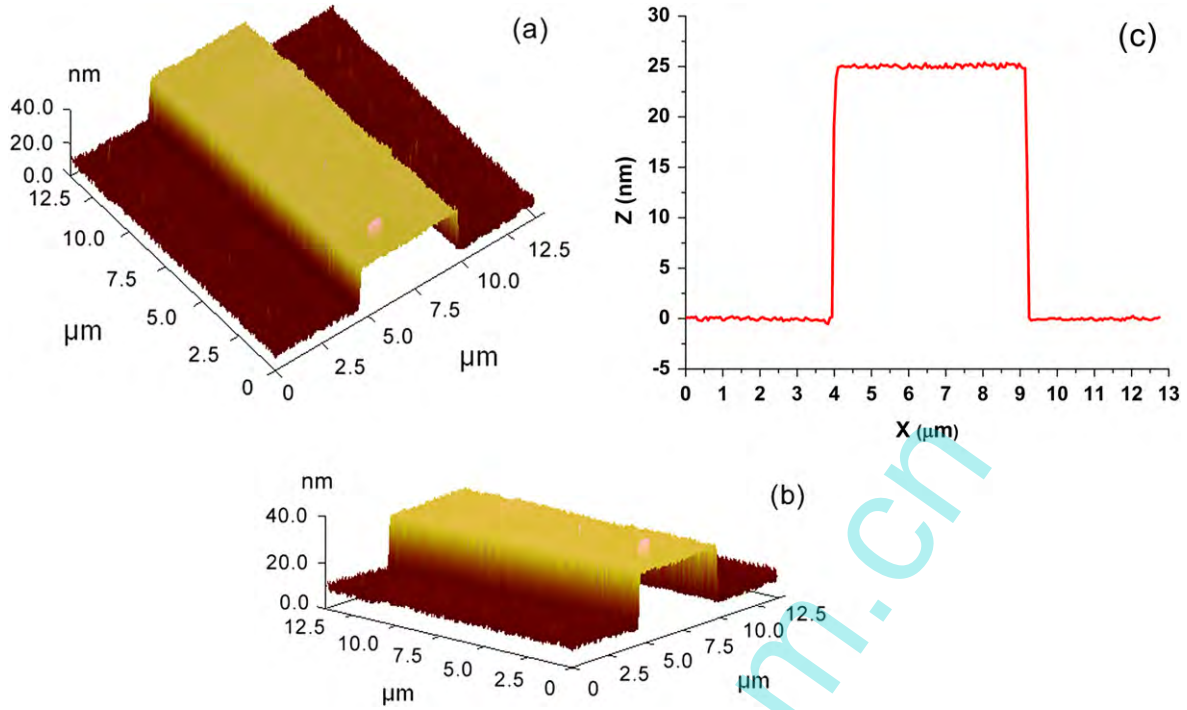

Figure 8. AFM images of (a), (b) three-dimensional configuration, and (c) line scan across the Au stripe on P(MMA-GMA) lower cladding.

the AFM image recorded on a $13 \times 13\ \mu m^2$ area to examine the detailed morphology. A better waveguide configuration with steep sidewalls is confirmed by figures 8(a) and (b) at different viewing angles. Though wet etching is typically isotropic, no obvious over etching on sidewalls is observed, which can effectively restrain the scattering loss. The protuberance on the metal stripe surface is the remains of photoresist that can be removed by further development. Imperfect edges of Au stripe are caused by the error of UV lithography and development, which can be lessened by improving equipment performances. The line scan across the Au stripe shown in figure 8(c) presents a quasi-rectangular cross-section view and a film thickness of about 25 nm, which is favorable for mode field control.

Since the cross-setional state of the LRSPP waveguide after slicing will affect the excition of the LRSPP mode, it was characterized by an SEM image after slicing, as shown in figure 9. The height of the Au stripe is about 25 nm. Though the image is a little blurred because of the charging effect of the thick polymer layers, it presents a distinct interface between the Au stripe and P(MMA-GMA) claddings. No remarkable roughness of the Au stripe is observed, which is favorable to reducing the coupling loss caused by scattering, while enhancing the excition of the LRSPP mode.

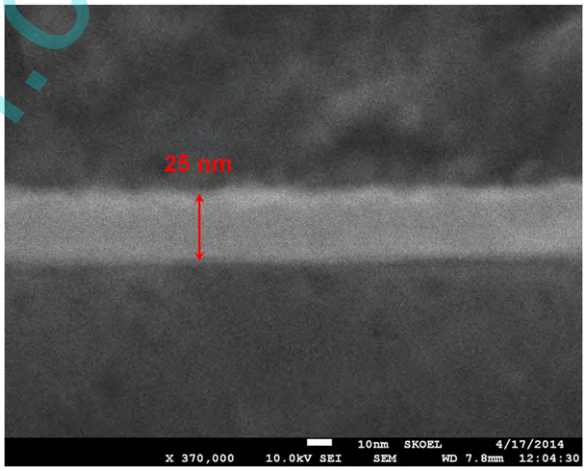

Figure 9. Cross-sectional SEM image of the fabricated Au stripe.

4. Results and discussion

4.1. Light output

The mode size of LRSPP waveguides can be adjusted by optimizing the cladding thickness and metal stripe dimensions to match that of the optical fiber. This offers low coupling loss, which is a key issue for the application of optical interconnects. Figure 10 shows the far-field light output of the fundamental mode from a 4 μm wide straight LRSPP waveguide at 1550 nm. No significant processing-induced light spreading is observed. The captured mode has no spike intensity of side modes originating from the sidewall roughness of the metal stripe or the RI nonuniformity of P(MMA-GMA) cladding. Before reaching the output port, nearly all light coupled from the input fiber to claddings has vanished while propagating along the waveguide. Besides, high order modes of LRSPP will cut off when the dimensions of the metal stripe satisfy certain conditions. Therefore, only the LRSPP mode, which is bound to the metal stripe, can be observed.

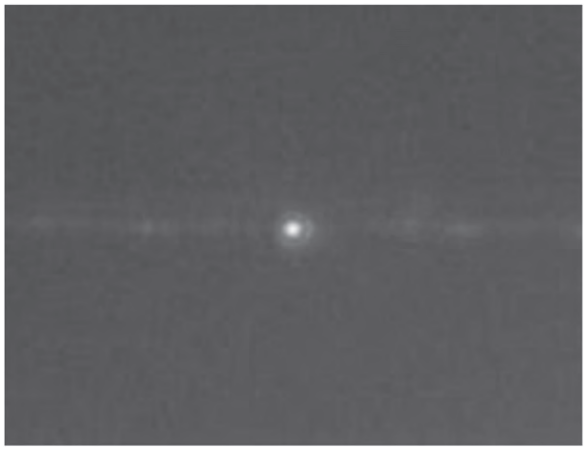

Figure 10. Far-field light output of a 4 μm wide metal stripe waveguide at 1550 nm.

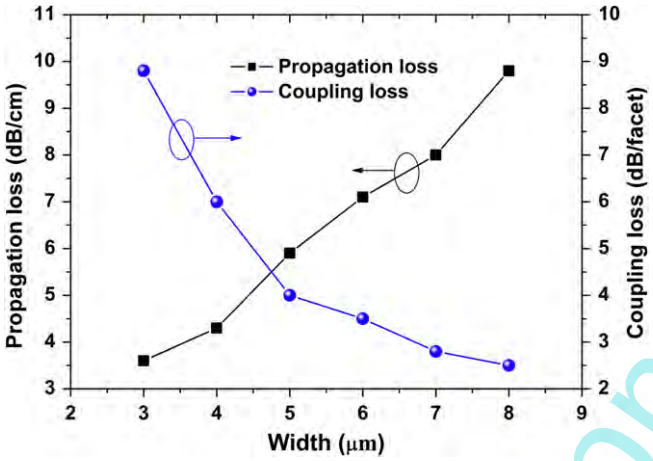

Figure 11. Measured propagation loss and coupling loss for different fabricated metal stripes with widths ranging from 3 to 8 μm in 1 μm increments.

4.2. Insertion loss

The insertion loss of LRSPP waveguides mainly includes the propagation loss of the Au stripe and the coupling loss between the fiber and the LRSPP waveguide. Supposing the integrity and facets of the waveguide were virtually the same in the experiment, the propagation loss and coupling loss depending on metal stripe widths for a 25 nm thick Au stripe waveguide measured by the cut-back method is shown in figure 11. With the increasing of the metal stripe width, the propagation loss improves from the lowest value of 3.6 dB cm^{-1} for a 3 μm wide straight waveguide to the highest value of 10.6 dB cm^{-1} for a 8 μm wide straight waveguide. Accordingly, the coupling loss decreases from 8.8 to 4 dB/facet with the increasing of waveguide width. The results clearly demonstrate that the propagation loss decreases as the metal stripe width narrows. This can be explained by considering that the optical field spreads out more into the polymer cladding with the reduction of stripe width instead of propagating along the lossy metal stripe. As a matter of fact, we have to face a tradeoff between the propagation loss and coupling loss, which means a decline in propagation loss accompanies an increment in coupling loss and vice versa. Though fewer field distributions occur inside the metal stripe as it becomes more narrow, narrower stripes cause a lower propagation loss and weaker mode confinement, while extending into the cladding, which leads to a larger coupling loss. Thus, the coupling loss affects the insertion loss highly for a narrower LRSPP waveguide.

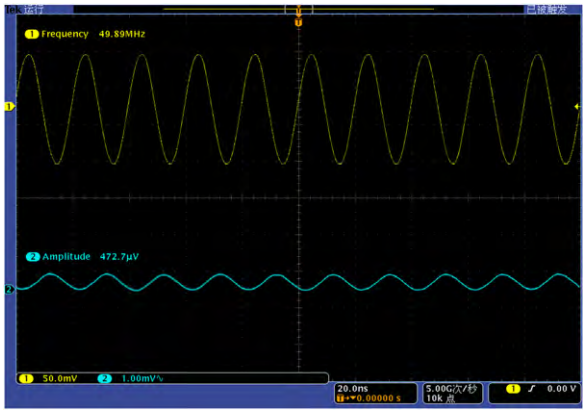

Figure 12. Measured sinusoidal modulated signal transmitting through a 4 μm wide LRSPP waveguide at a frequency of 49.89 MHz.

4.3. Optical transmissions

According to the measurement setup in figure 2, the optical signal (Channel 2) is measured by an oscilloscope that collects the output optical power transmitted through a 4 μm wide LRSPP waveguide at a wavelength of 1550 nm. This occurs when a 49.89 MHz sinusoidal electrical modulating signal (Channel 1) is applied to the lithium niobate electro-optic modulator, as shown in figure 12. In spite of obstacles of longitudinal oscillations of electrons, wave vector difference, dispersion, and loss, the transmission of a light signal through the LRSPP waveguide is confirmed. The low optical intensity in Channel 2 results from the attenuated optical power due to the 21 dB insertion loss of this 2 cm long LRSPP waveguide. By all accounts, the LRSPP waveguide is a potential solution to optical interconnects and other functional devices.

5. Conclusions

The fabrication of Au stripe LRSPP waveguides by wet chemical etching technology has been investigated. Our studies of morphological and structural characteristics of Au stripes show that no obvious evaporation spits or metal wings exist along the edges of the stripe. The steep sidewalls provide good mode field control, which has been proven by the IR photo of field pattern. The light guiding and routing along Au stripes embedded in P(MMA-GMA) claddings has been investigated. Optical characteristics of propagation loss, coupling loss, and signal transmission at the telecom wavelength are demonstrated. Experimental results indicate that

the proposed fabrication process is an efficient and reliable method to construct LRSPP waveguides with low propagation loss.

Acknowledgement

This work is supported by the National Natural Science Foundation of China (Nos. 61177027, 61107019, 61205032 and 61261130586), Science and Technology Development Plan of Jilin Province (No. 20140519006JH), Program for Special Funds of Basic Science & Technology of Jilin University (Nos. 201100253 and 201103071), China Postdoctoral Science Foundation (No. 2012M510900).

References

[1] Casper B, Balamurugan G, Jaussi J E, Kennedy J, Mansuri M, O'Mahony F and Mooney R 2007 Future microprocessor interfaces: analysis, design and optimization *Proc. IEEE Custom Integrated Circuits Conf.* (San Jose, CA) pp 479–86

[2] Li Y P and Henry C H 1996 Silica-based optical integrated circuits *IEE Proc.-Optoelectron.* **143** 263–80

[3] Ridder R M, Worhoff K, Driessen A, Lambeck P V and Albers H 1998 Silicon oxynitride planar waveguiding structures for application in optical communication *IEEE J. Sel. Top. Quant. Electron.* **4** 930–7

[4] Roelkens G *et al* 2014 Silicon-based photonic integration beyond the telecommunication wavelength range *IEEE J. Sel. Top. Quant. Electron.* **20** 8201511

[5] Chakraborty R, Ganguly P, Das S, Biswas J C and Lahiri S K 2000 Integrated optical waveguides in $LiNbO_3$: modeling and experimental analysis *Proc. SPIE* 4417, pp 278–85

[6] Eldada L A 2002 Polymer integrated optics: promise versus practicality *Proc. SPIE* **4642** 11–22

[7] Boltasseva A and Bozhevolnyi S I 2006 Directional couplers using long-range surface plasmon polariton waveguides *IEEE J. Sel. Top. Quant. Electron.* **12** 1233–41

[8] Nikolajsen T, Leosson K and Bozhevolnyi S I 2004 Surface plasmon polariton based modulators and switches operating at telecom wavelengths *Appl. Phys. Lett.* **85** 5833–5

[9] Sakaidani T, Fujii G, Fujikake A, Namekata N, Fukuda D and Inoue S 2012 Mach-Zehnder interferometer using a long-range surface plasmon polariton waveguide coupler *Proc. SPIE* **8457** 845722

[10] Jiang J, Callender C L and Jacob S 2012 Long-period gratings based on surface plasmon polariton waveguides in fluorinated polymer *IEEE Photonic. Tech. Lett.* **24** 2169–71

[11] Park S and Song S H 2006 Polymeric variable optical attenuator based on long range surface plasmon polaritons *Electron. Lett.* **42** 402–4

[12] Zhang T, Qian G, Wang Y Y, Xue X J, Shan F, Li R Z, Wu J Y and Zhang X Y 2014 Integrated optical gyroscope using active Long-range surface plasmon-polariton waveguide resonator *Scientific Reports* **4** 3855

[13] Kim J T, Ju J J, Park S, Kim M S, Park S K and Lee M H 2008 Chip-to-chip optical interconnect using gold long-range surface plasmon polariton waveguides *Opt. Express* **16** 13133

[14] Nikolajsen T, Leosson K, Salakhutdinov I and Bozhevolnyi S I 2003 Polymer-based surface-plasmon-polariton stripe waveguides at telecommunication wavelengths *Appl. Phys. Lett.* **82** 668–70

[15] Boltasseva A, Nikolajsen T, Leosson K, Kjaer K, M Larsen M S and Bozhevolnyi S I 2005 Integrated optical components utilizing long-range surface plasmon polaritons *IEEE J. Lightwave Technol.* **23** 413–22

[16] Takahara J and Miyata M 2013 Mutual mode control of short-and long-range surface plasmons *Opt. Express* **21** 27402–10

[17] Charbonneau R and Berini P 2000 Experimental observation of plasmon-polariton waves supported by a thin metal film of finite width *Opt. Lett.* **25** 844–6

[18] Berini P 2000 Plasmon-polariton waves guided by thin lossy metal films of finite width: bound modes of symmetric structures *Phys. Rev.* B **61** 10484–503

[19] Charbonneau R, Lahoud N, Mattiussi G and Berini P 2007 Characteristics of ultra-long range surface plasmon waves at optical frequencies *Opt. Express* **15** 977–84

[20] Mattiussi G, Lahoud N, Charbonneau R and Berini P 2005 Integrated optics devices for long ranging surface plasmons: fabrication challenges and solutions *Proc. SPIE* **5720** 173–86

[21] Kim J T, Park S, Ju J J, Park S K, Kim M S and Lee M H 2007 Low-loss polymer-based long-range surface plasmon-polariton waveguide *IEEE Photon. Technol. Lett.* **19** 1374–6

[22] Kim J T, Park S, Park S K, Kim M S, Lee M H and Ju J J 2009 Gold stripe sptical waveguides fabricated by a novel double-layered liftoff process *ETRI J.* **31** 778–83

[23] Moazzez B, O'Brien S M and Merschrod S E F 2013 Improved adhesion of gold thin films evaporated on polymer resin: applications for sensing surfaces and MEMS *Sensors* **13** 7021–32

[24] Li W T, Charters R B, Luther-Davies B and Mar L 2004 Significant improvement of adhesion between gold thin films and a polymer *Appl. Surf. Sci.* **233** 227–33

[25] Patsis G P, Gogolides E and Werden K V 2005 Effects of photoresist polymer molecular weight and acid-diffusion on line-edge roughness *Jpn. J. Appl. Phys.* **44** 6341–8

[26] Fan H, Skrzek E L and Berini P 2011 Measurement of long-range surface plasmon-polariton devices in Cytop *Proc. SPIE* **8007** 800706

[27] Fei X, Fu N, Wang Y, Hu J, Cui Z C, Zhang D M, Ma C X, Liu S Y and Yang B 2006 Synthesis and characterization of crosslinkable poly(MMA-co-GMA) and its application in arrayed waveguide grating *Chem. J. Chinese* U. **27** 571–4

[28] Noh Y-O, Lee C-H, Kim J-M, Hwang W-Y, Won Y-H, Lee H-J, Han S-G and Oh M-C 2004 Polymer waveguide variable optical attenuator and its reliability *Opt. Commun.* **242** 533–40

[29] Charbonneau R, Scales C, Breukelaar I, Fafard S, Lahoud N, Mattiussi G and Berini P 2006 Passive integrated wptics elements based on long-rrnge surface plasmon polaritons *IEEE J. Lightwave Tech.* **24** 477–94

[30] Brandt T, Hövel M, Gompf B and Dressel M 2008 Temperature- and frequency-dependent optical properties of ultrathin Au films *Phys. Rev.* B **78** 205409

[31] Zhang Q G, Zhang X, Cao B Y, Fujii M, Takahashi K and Ikuta T 2006 Influence of grain boundary scattering on the electrical properties of platinum nanofilms *Appl. Phys. Lett.* **89** 114102

[32] Rossnagel S M and Kuan T S 2004 Alteration of Cu conductivity in the size effect regime *J. Vac. Sci. Technol.* B **22** 240–7

[33] Mehmood T, Kaynak A, Dai X J, Kouzani A, Magniez K, de Celis D R, Hurren C J and du Plessis J 2014 Study of oxygen plasma pre-treatment of polyester fabric for improved polypyrrole adhesion *Mater. Chem. Phys.* **143** 668–75